Front. Chem. China 2010, 5(2): 171–177
DOI 10.1007/s11458-010-0111-y

RESEARCH ARTICLE

Photo-induced electron transfer study of rhenium(I) bipyridyl complexes with covalently linked phenothiazine donor through different bridge

Shiguo SUN (✉)[1], Lei SHI[1], Fengyu LIU[1,2,3], Jiangli FAN[1] and Xiaojun PENG (✉)[1]

A novel rhenium(I) bipyridyl complex 1a, [(4,4'-di-COOEt-bpy)Re(CO)$_3$(py-NHCO-PTZ)PF$_6$] and a model 1b, [(4,4'-di-COOEt-bpy)Re(CO)$_3$(py-PTZ)PF$_6$] (bpy is 2, 2'-bipyridine, py-NHCO-PTZ is phenothiazine-(10-carbonyl amide) pyridine and py-PTZ is 10-(4-picolyl) phenothiazine) were synthesized. Their photo-induced electron transfer (ET) reaction with electron acceptor methyl viologen (MV^{2+}) in acetonitrile was studied by nanosecond laser flash photolysis at room temperature. Photoexcitation of 1 in the presence of MV^{2+} led to ET from the Re moiety to MV^{2+} generating Re(II) and methyl viologen radical ($MV^{\bullet+}$). Then Re(II) was reduced either by the charge recombination with $MV^{\bullet+}$ or by intramolecular ET from the attached PTZ, regenerating the photosensitizer Re(I) and forming the PTZ radical at 510 nm. In the case of 1b, the absorption for PTZ radical can be observed distinctly accompanied intermolecular ET, whereas not much difference at 510 nm can be detected for 1a on the time scale of the experiments. This demonstrates that the linking bridge plays a key role on the intramolecular ET in complex 1.

Keywords rhenium(I) bipyridyl complex, intermolecular electron transfer, intramolecular electron transfer, phenothiazine, acceptor

1 Introduction

Photo-induced electron transfer (ET) plays an important role in a variety of chemical, biologic, and physical processes; a number of models have been constructed to study the ET pathway and mechanism.

One of the simplest representative models is a dyad or triad system that consists of electron donor and electron acceptor; usually, a tyrosine or manganese complex covalently linked with a ruthenium(II) bipyridyl complex is used as electron donor and methyl viologen (MV^{2+}) as electron acceptor [1–7]. Unfortunately, the absorption of tyrosine radical is very weak (λ_{max} = 410 nm, ε = 3000 L·mol^{-1}·cm^{-1}) [8–10] and overlapped with that of the MV^{2+} radical ($MV^{\bullet+}$) (λ_{max} = 398 nm, ε = 42000 L·mol^{-1}·cm^{-1}, λ_{max} = 600 nm, ε = 13900 L·mol^{-1}·cm^{-1}). Therefore, some special techniques, for example, electron paramagnetic resonance (EPR), etc., must be utilized for its characterization. It is also the case for the manganese complexes' characterization [1–7]. It is noted that the absorption of the phenothiazine (PTZ) radical (λ_{max} = 510 nm, ε = 10000 L·mol^{-1}·cm^{-1}) is far away from that of the $MV^{\bullet+}$, which can be conveniently monitored by spectrometry measurements. In addition, PTZ has a higher outer sphere one-electron oxidation potential and hence it was a suitable electron donor [11–15]. On the other hand, the Re(II/I) oxidation potentials are significantly positive, which could provide a larger ET driving force than the ruthenium(II) bipyridyl complexes [16]. All these features suggest that PTZ and Re(II/I) could form a good pair of partners for ET process. Moreover, it would be interesting to examine the ET process in PTZ-rhenium(I) pair in comparison with the donor-acceptor interaction in tyrosine or manganese complex-ruthenium(II) bipyridyl complex in the above mentioned model system.

As shown in Scheme 1, [(4,4'-di-COOEt-bpy)Re(CO)$_3$(py-PTZ) PF$_6$] (**1b**) can be considered as a good model complex, and its intramolecular ET process has been studied by Meyer et al. [11–15]. It is suggested that the initial excitation of the metal-to-ligand charge transfer (MLCT) excited state was followed by rapid intramolecular ET quenching to yield the charge separated excited state [bpy$^{\bullet+}$-Re-PTZ$^{\bullet+}$]$^+$ (PTZ radical), which decayed to the ground state by backward intramolecular ET mainly through space because the center to center distance between (4,4'-di-COOEt-bpy$^{\bullet+}$) and PTZ$^{\bullet+}$ can vary from ~6 to ~9 Å. The PTZ donor can be adapted to a much favorable configuration through the rotation around –CH$_2$– bridge due to its flexibility [11–15]. To further figure out the real function for the flexible –CH$_2$– bridge during the ET process, a potential approach is to replace the –CH$_2$– bridge in **1b** by the –CONH– bridge as shown in **1a**. The reason is that the amide bond is relative rigid and has a considerable double bond property due to the lone pair

Received December 29, 2009; accepted February 21, 2010
1. State Key Laboratory of Fine Chemicals, Dalian University of Technology, Dalian 116012, China
2. Department of Chemistry, Dalian University of Technology, Dalian 116024, China
3. State Key Laboratory of Bioelectronics, Southeast University, Nanjing 210096, China
E-mail: shiguo@dlut.edu.cn, pengxj@dlut.edu.cn

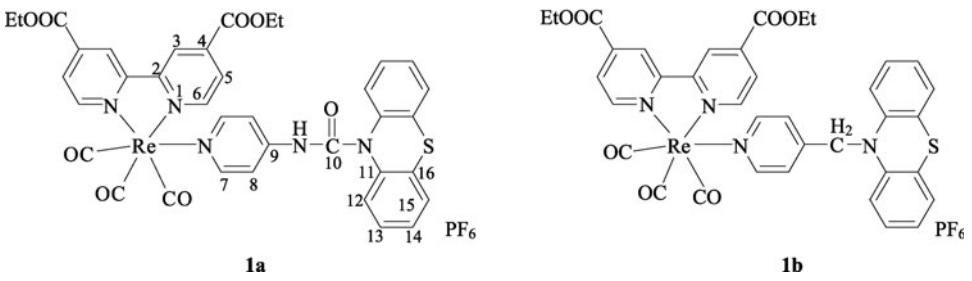

Scheme 1 The structure of [(4,4'-di-COOEt-bpy)Re(CO)$_3$(py-NHCO-PTZ)PF$_6$] (**1a**) and [(4,4'-di-COOEt-bpy)Re(CO)$_3$(py-PTZ) PF$_6$] (**1b**).

electrons on nitrogen delocalizing into the carbonyl group, which is often used as a neutral bridge to attach other structure subunit and hence the conformation can be fixed to some extent. As far as we know, no work has been done on the photo-induced ET reaction of Re moiety and MV^{2+} system. In the article, we reported the synthesis of **1a**, and its photo-induced ET reaction with electron acceptor MV^{2+} was investigated in comparison with that of **1b** by using nanosecond laser flash photolysis. Here, we would like to report some preliminary results concerning the ET processes.

2 Experimental

2.1 General

NMR spectra were obtained on a Varian INOVA 400 MHz spectrometer using TMS as internal standard. The electrospray ionization mass spectrometer (ESI-MS) experiments were performed on a HP1100 LC/MSD. HRMS were detected on a Q-Tof Micromass spectrometer (Manchester, England). The absorption spectra were recorded on an HP 8453 spectrophotometer, and the emission spectra were recorded using a PTI-C-700 fluorometer. The nanosecond laser flash photolysis was detected on an Edinburgh Instruments Ltd. LP920 Laser Flash Photolysis Spectrometer using a frequency tripled Q-switched Nd:YAG laser, 355 nm wavelength, 8 ns flashes, the average energy of the laser pulses was 1 mJ, and the detecting method has been described [17].

2.2 Materials

4,4'-dimethyl-2,2'-bipyridine, $Re(CO)_5Cl$, ammonium hexafluorophosphate (NH_4PF_6), $AgPF_6$, and phenothiazine-10-carbonyl chloride were purchased from Aldrich. The MV $(PF_6)_2$ was prepared by the reaction of 4,4'-bipyridine and CH_3I. Aqueous NH_4PF_6 solution was added to precipitate the PF_6 salt, and the product was purified by recrystallization from C_2H_5OH. Intermediates 4,4'-dicarboxyl-2,2'-bipyridine (**3**) and 4,4'-bis(ethoxycarbonyl)-2,2'-bipyridine (**4**) were prepared according to Ref. [18]. The silica gel (200–300 mesh) used for column chromatography was bought from Qingdao Ocean Chemical Factory, China. Other chemicals and solvents were all of reagent grade for synthesis and used as received.

2.3 Phenothiazine-(10-carbonyl amide) pyridine (py-NHCO-PTZ) (**6**)

As shown in Scheme 2, 2.1 mmol of phenothiazine-10-carbonyl chloride, 2.0 mmol of 4-aminopyridine, and 4.3 mmol of triethyl amine were dissolved in 30 mL of dry acetonitrile, and the solution was stirred for 10 h at room temperature. Then, 20 mL of H_2O was added to the solution, and the solution was extracted with chloroform (20 mL) three times. The organic phase was collected and evaporated to dryness. The crude products were purified by column chromatography on silica gel (CH_3CH_2OH:CH_2Cl_2 = 1:30), and 312 mg white crystals were obtained. The yield for **6** was 49%. ^{1}H NMR (δ ppm, DMSO-d_6): 7.30 (t, 2H, J = 7.6 Hz, H_9), 7.39 (t, 2H, J = 7.6 Hz, H_8), 7.49 (d, 2H, J = 6.3 Hz, H_2), 7.53 (dd, 2H, J = 7.6 Hz, 1.0 Hz, H_{10}), 7.72 (dd, 2H, J = 8.1 Hz, 1.0 Hz, H_7), 8.35 (d, 2H, J = 6.2 Hz, H_1), 9.03 (s, 1H, H_4); ^{13}C NMR (δ ppm, DMSO-d_6):113.59 (C_2), 126.38 (C_7), 126.50 (C_9), 127.42 (C_8), 127.81 (C_{10}), 131.95 (C_{11}), 138.29 (C_6), 146.36 (C_1), 151.42 (C_5); ESI-MS Positive: $[M + H]^+$ (*m/z* 320.1).

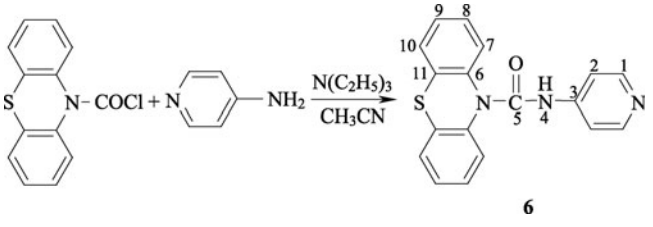

Scheme 2 Synthetic route for the intermediate **6**.

2.4 10-(4-picolyl)phenothiazine (py-PTZ) (**7**)

Compound **7** was prepared according to Ref. [13]. ESI-MS Positive: $[M + H]^+$ (*m/z* 291.1).

2.5 Synthesis of **1a**

Complex **1a** was prepared according to a modification of the method described by Schanze et al. [19]. As shown in Scheme 3, 1 mmol of $Re(CO)_5Cl$ and 1 mmol of **4** were dissolved in 150 mL of toluene. The solution was refluxed for 1 h, and then the solvent was evaporated under a vacuum. An orange solid residue of crude **5** was obtained. It was redissolved in ethanol (20 mL) without purification, and 1.5 mmol of $AgPF_6$ together with 1.5 mmol of **6** were added. The mixture was refluxed for 1 h, and then ethanol was evaporated. The residue were redissolved in 50 mL of CH_2Cl_2 and then filtrated. The solvent was evaporated to dryness. Purification was made using column chromatography on silica gel using CH_2Cl_2: CH_3COCH_3 (50∶1) as eluent. The yield of **1a** was 91%. ^{1}H NMR (δ ppm, Acetone-d_6): 1.43 (t, 6H, J = 7.1 Hz, $-OCH_2CH_3$), 4.51 (q, 4H, J = 7.1 Hz, $-OCH_2CH_3$), 7.29 (t, 2H, J = 7.6 Hz, H_{14}, $H_{14'}$), 7.37 (t, 2H, J = 7.6 Hz, H_{13}, $H_{13'}$), 7.48 (d, 2H, J = 5.8 Hz, H_8, $H_{8'}$), 7.50 (d, 2H, J = 7.6 Hz, H_{15}, $H_{15'}$), 7.71 (dd, 2H, J = 8.0 Hz, 1.0 Hz, H_{12}, $H_{12'}$), 8.23 (d, 2H, J = 5.8 Hz, H_7, $H_{7'}$), 8.39 (dd, 2H, J = 5.6 Hz, 1.5 Hz, H_5, $H_{5'}$), 9.22 (s, 2H, H_3, $H_{3'}$), 9.66 (d, 2H, J = 5.6 Hz, H_6, $H_{6'}$); ^{13}C NMR (δ ppm, Acetone-d_6): 14.35 ($-OCH_2CH_3$), 63.66 ($-OCH_2CH_3$), 116.28 (C_8, $C_{8'}$), 125.35 (C_3, $C_{3'}$), 127.66 (C_{12}, $C_{12'}$), 128.07 (C_{14}, $C_{14'}$), 128.57 (C_{13}, $C_{13'}$), 128.94 (C_{15}, $C_{15'}$), 129.01 (C_5, $C_{5'}$), 133.90 (C_{16}, $C_{16'}$), 138.85 (C_{11}, $C_{11'}$), 142.89 (C_4, $C_{4'}$), 150.54 (C_9), 151.65 (C_{10}), 153.02 (C_7, $C_{7'}$), 156.08 (C_6, $C_{6'}$), 157.57 (C_2, $C_{2'}$), 163.73 (–COO–), 187.89 (CO), 191.79 (CO), 196.31 (CO); ESI-MS Positive: $[M\text{-}PF_6]^+$ (*m/z* 890.1); HRMS calcd. for $C_{37}H_{29}N_5O_8ReS$ 890.1294 found 890.1308.

2.6 Synthesis of **1b**

Complex **1b** was prepared according to the same procedure as **1a**, except that **7** was used as ligand to replace **6**. Purification was made by column chromatography on silica gel using CH_2Cl_2∶CH_3COCH_3 (70∶1) as eluent. The yield for **1b** was 90%. ^{1}H NMR (δ ppm, $CDCl_3$): 1.49 (t, 6H, J = 7.2 Hz, $-OCH_2CH_3$), 4.55 (q, 4H, J = 7.2 Hz, $-OCH_2CH_3$), 5.00 (s, 2H, H_{10}), 6.52 (d, 2H, J = 8.2 Hz, H_{12}, $H_{12'}$), 6.88 (t, 2H, J = 7.6 Hz, H_{14}, $H_{14'}$), 6.99 (dd, 2H, J = 7.6 Hz, 1.2 Hz, H_{13}, $H_{13'}$), 7.10 (dd, 2H, J = 7.6 Hz, 1.2 Hz, H_{15}, $H_{15'}$), 7.41 (d, 2H, J = 6.2 Hz, H_8, $H_{8'}$), 8.02 (d, 2H, J = 6.2 Hz, H_7, $H_{7'}$), 8.27 (dd, 2H, J = 5.6 Hz, 1.2 Hz, H_5, $H_{5'}$), 8.93 (s, 2H, H_3, $H_{3'}$), 9.22 (d, 2H, J = 5.6 Hz, H_6, $H_{6'}$); ^{13}C NMR (δ ppm, $CDCl_3$):14.30 ($-OCH_2CH_3$), 50.57 (C_{10}), 63.70 ($-OCH_2CH_3$), 115.73 (C_{12}, $C_{12'}$), 123.38 (C_{14}, $C_{14'}$), 124.58 (C_{16}, $C_{16'}$), 125.08 (C_3, $C_{3'}$), 126.11 (C_8, $C_{8'}$), 127.52(C_{15}, $C_{15'}$), 127.86 (C_{13}, $C_{13'}$), 128.66 (C_5, $C_{5'}$), 142.61 (C_4, $C_{4'}$), 144.06 (C_{11}, $C_{11'}$), 151.54 (C_7, $C_{7'}$), 152.59 (C_9), 153.77 (C_6, $C_{6'}$), 156.48 (C_2, $C_{2'}$), 162.53 (–COO–), 195.29 (CO), 198.43 (CO), 198.93 (CO); ESI-MS Positive: $[M\text{-}PF_6]^+$ (*m/z* 861.1); HRMS calcd. for $C_{37}H_{30}N_4O_7ReS$ 861.1393 found 861.1378.

3 Results and discussion

3.1 Synthesis of **1a** and **1b**

The synthesis of complex **1** was accomplished by using a modified literature procedure [19]. Oxidation of 4,4'-dimethyl-2,2'-bipyridine **2** afforded the diacids **3** in 92% yield, which was then cleanly converted to **4** in 93% yield with absolute ethanol. After refluxing a mixture of $Re(CO)_5Cl$ and **4** in toluene for 1 h, the rhenium complex **5** was obtained as an orange solid. Without further purification, **5** was reacted directly with different PTZ ligands **6** or **7** in ethanol, resulting in the corresponding complex **1a** and **1b** in good yield.

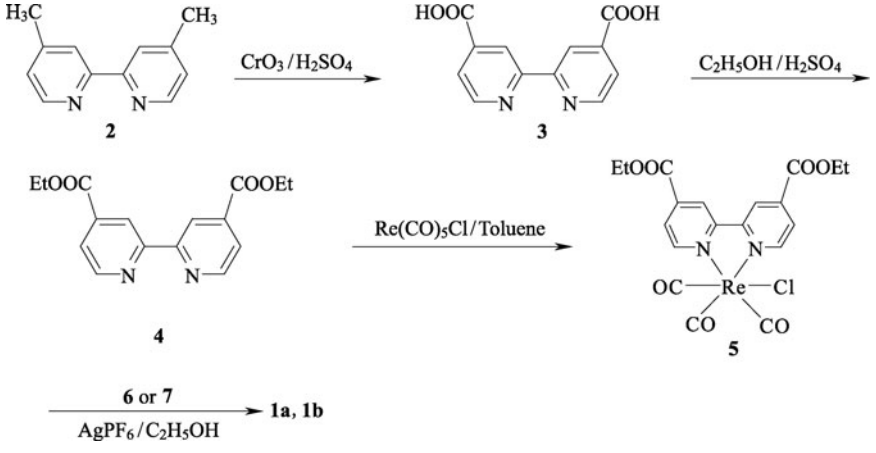

Scheme 3 Synthetic route for the complex **1a** and **1b**.

3.2 Absorption and emission

Normalized absorption and emission spectra of 10 μmol·L^{-1} **1a** and **1b** are shown in Figure 1. Both **1a** and **1b** showed typical absorption patterns for the rhenium(I) bipyridyl complex [3]. In comparison with **1b**, **1a** exhibited a red shift of 7 nm and 40 nm in MLCT absorption maximum and emission maximum, and a red shift of 37 nm for the bipyridine based $\pi_L \rightarrow \pi_L^*$ absorption maximum, respectively. At room temperature, the emission intensity of **1a** was much weaker than that of **1b**. The emission lifetime measurement by time correlated single photon counting showed a biexponential process with two time constants of 0.3 ns (83.5%) and 20 ns (16.5%) for **1a**, 1.2 ns (92.4%) and 121 ns (7.6%) for **1b**, and the radiative decay rate constants k_r (determined from the ratio of the emission quantum yield and lifetime, $k_r = \Phi_{em}/\tau_{em}$) for the faster component was 3.3×10^5 s^{-1} for **1a** and 1.2×10^5 s^{-1} for **1b**, respectively, indicating a faster quenching of the rhenium-based ^{3}MLCT excited state owing to the delocalization of the lone pair electrons on nitrogen and the extended π-conjugation provided by the –CONH– bridge.

3.3 Nanosecond laser flash photolysis

The time-resolved transient absorption of 100 μmol·L^{-1} complex **1** with 150 equiv. of MV^{2+} as an electron acceptor in dry acetonitrile after the irradiation of 355 nm laser pulse (8 ns, 1 mJ/pulse) are shown in Figure 2.

The two peaks appeared at 398 and 600 nm are assigned to the typical absorption of $MV^{\bullet+}$ radical [8–10], and the peak appeared at 510 nm in **1b** is assigned to the absorption of PTZ radical $[bpy^{\bullet+}\text{-Re-PTZ}^{\bullet+}]^+$ according to literature [11–15]. It demonstrated that complex **1b** absorbed light energy and reached MLCT excited state $[bpy\text{-}Re^{+}\text{-PTZ}]^*$, which can transfer an electron to MV^{2+} in a bimolecular reaction, resulting in the formation of oxidized Re(II) and the $MV^{\bullet+}$ radical. The PTZ donor provided an electron to the oxidation state Re^{2+} through an intramolecular ET process to form a

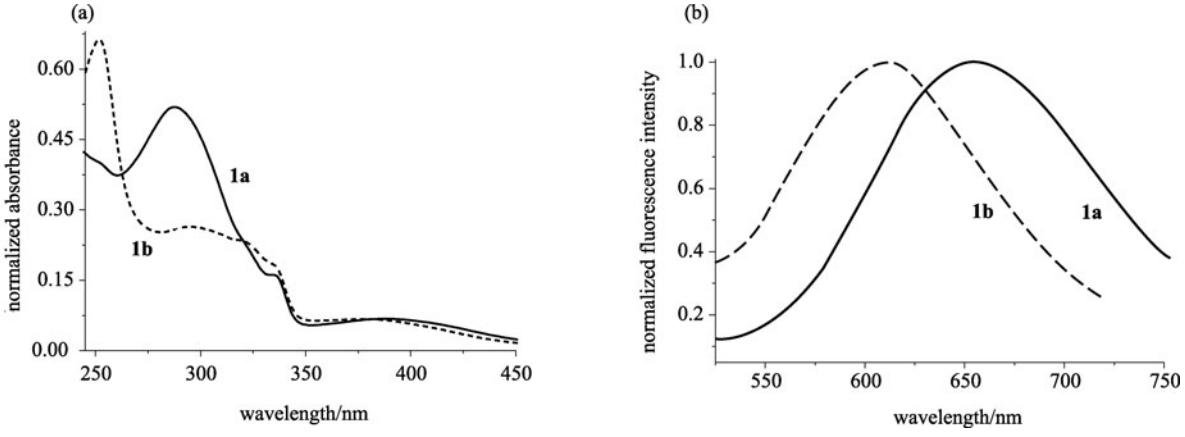

Figure 1 Normalized (a) absorption and (b) emission spectra of 10 μmol·L^{-1} **1a** and **1b** in dry acetonitrile at room temperature.

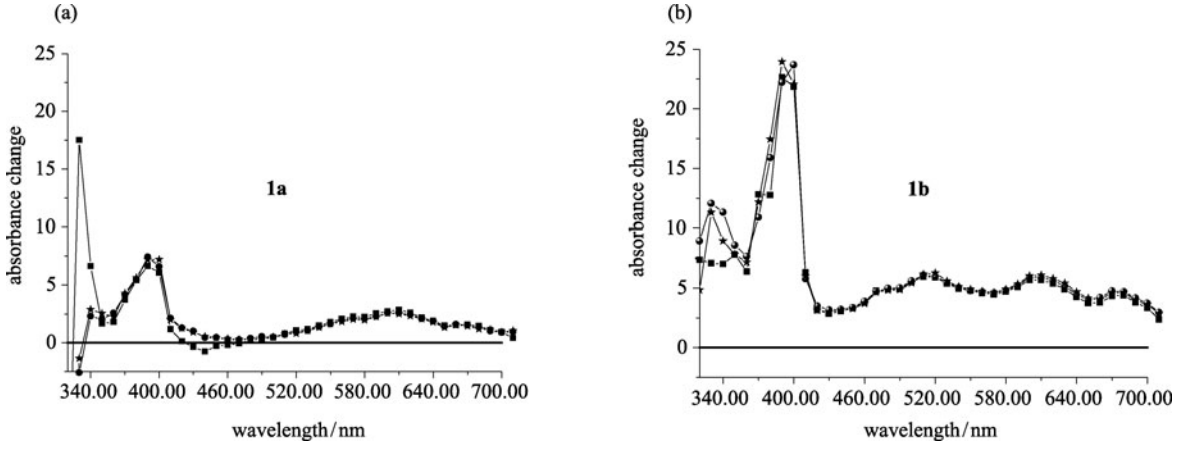

Figure 2 Time-resolved absorption spectra of 100 μmol·L^{-1} **1** ((a) **1a**; (b) **1b**) in the presence of 150 equiv. of MV^{2+} in dry acetonitrile at room temperature; the spectra were recorded at delays of 100(■), 200(●), and 300(♦) ns following 355 nm excitation.

PTZ radical, which was then returned to the ground-state through charge recombination route **II** as shown in Scheme 4.

The $MV^{\bullet+}$ radical decayed via charge recombination with both oxidized PTZ (route **II**) and rhenium species (route **I**) and route **II** is a rate controlling (limiting step) process because intramolecular ET rate is much faster than intermolecular charge recombination rate, and $[bpy^{\bullet+}\text{-Re-PTZ}^{\bullet+}]^{+}$ in route **II** possesses a lower energy level than $[bpy\text{-Re-PTZ}]^{2+}$ in route **I**.

However, in the case of **1a**, the PTZ radical's absorption can not be observed at 510 nm like that in **1b** in Figure 2, so the transient absorbance kinetics at 510 nm for 100 μmol·L^{-1} complex **1** with and without the presence of 150 equiv. of MV^{2+} was studied in Figure 3. As reported [11–15], **1b** alone can be photo-induced to the MLCT excited state, followed by rapid intramolecular ET quenching to give the charge separated excited state PTZ radical $[bpy^{\bullet+}\text{-Re-PTZ}^{\bullet+}]^{+}$, then decayed to the ground state through backward intramolecular ET. The kinetic decay at 510 nm was fitted well by a single exponential process with a lifetime of 11 ns for **1b** alone, which is in good agreement with the literature's data [11–15].

An intense build up can be observed for **1a** alone, which originates from the formation and decay of the MLCT excited state. The kinetic decay curve at 510 nm was fitted by a biexponential process with two time constants (11 ns (4%) and 13 μs (96%)). The faster recovery (4%) rate constant agreed well with that of **1b**, which is very likely due to the MLCT excited state decay. The slower recovery (96%) rate constant is from decay of the PTZ radical. According to Meyer's work [11–15], there were several processes leading to the formation of the PTZ radical for **1b** alone, such as intramolecular quenching of the ^{3}MLCT state, electron transfer quenching of the ^{1}MLCT state, photo ejection of an electron from PTZ followed the laser power (1 mJ/pulse) used, and so on. While for **1a** alone, energy transfer quenching and photo ejection of an electron from PTZ could be the main route to generate the PTZ radical, because the existing –CONH– bridge stabilized PTZ radical to some extent due to the extended π-system conjugation, which may contribute to the explanation of the above-mentioned intense build up. After addition of MV^{2+} into the acetonitrile solution of **1a**, only the transient absorption of $MV^{\bullet+}$ radical can be detected. It means that the photo excitation of **1a** led to ET from the Re moiety to MV^{2+}, but the photo oxidized Re(II) cannot be reduced by the attached PTZ intramolecularly, that is, the –CONH– bridge inhibits intramolecular ET in **1a**, so no absorption can be observed at 510 nm in Figure 2. On the contrary, an intense build up at 510 nm from PTZ radical can be measured after MV^{2+} was added into the solution of **1b**, and the decay curve could not be exponentially fitted because it was waved heavily, which proved that intramolecular ET could take place concomitantly with intermolecular ET for **1b**.

The subsequent recombination to generate the ground-state

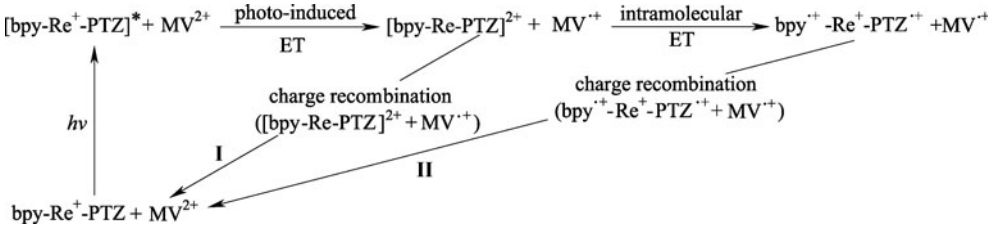

Scheme 4 Schematic routes for the photo-induced ET process between **1b** and MV^{2+}.

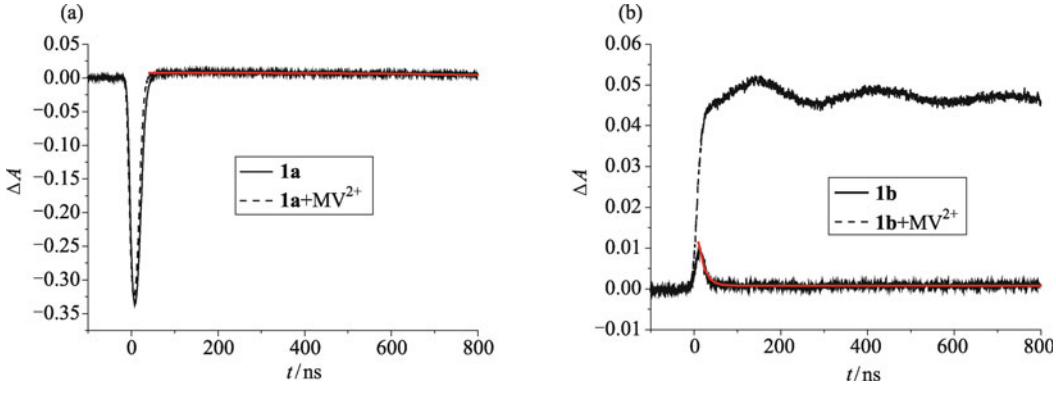

Figure 3 Transient absorption kinetics detected at the $PTZ^{\bullet+}$ absorption maximum 510 nm for 100 μmol·L^{-1} (a) **1a** and (b) **1b** with and without the presence of 150 equiv. of MV^{2+} in dry acetonitrile, respectively. The red line is the exponential fitted result.

reactants has also been studied by monitoring the decay of the absorption of the formed $MV^{\bullet+}$ radical around 600 nm in Figure 4.

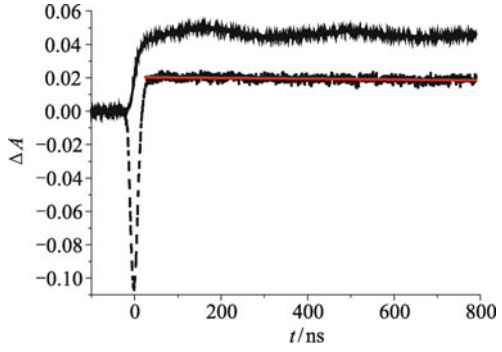

Figure 4 Transient absorption kinetics detected at the $MV^{\bullet+}$ absorption maximum 600 nm for 100 μmol·L^{-1} **1a** and **1b** with the presence of 150 equiv. of MV^{2+} in dry acetonitrile, respectively. The red line is the exponentially fitted result.

An intense buildup of the $MV^{\bullet+}$ radical was observed after the repeated flash. Although the kinetic decay in **1b** cannot be exponentially fitted because it was waved heavily, the decay rate is obviously slower than that in **1a**, which had a rate constant of 1.6×10^6 s^{-1}. The reason is that the $MV^{\bullet+}$ radical decayed to the ground state through both route **I** and **II** in the case of **1b**, and route **II** was predominant, as mentioned above, whereas only route **I** existed in the case of **1a** due to the absence of the PTZ radical.

3.4 Geometry-optimized structures

As suggested in literature [12–14], the intramolecular ET in **1b** is mainly through space since the PTZ donor can be adapted to a much favorable configuration for donor-acceptor electronic coupling through rotation around the $–CH_2–$ bridge. What makes such a big difference in **1a** after $–CH_2–$ is replaced by –CONH–? Has the configuration been changed so much that intramolecular ET cannot be realized through space? To further figure this out, the geometry-optimized structures of complex **1** for the ground state were calculated by using density functional theory (DFT) with LSDA function and the LanL2DZ basis set [20]. All calculations were performed with the Gaussian 09 program [21] without symmetry restriction. The HOMO and LUMO orbitals are illustrated in Figure 5.

As seen in the model of **1**a (Figure 5, left), the introduction of –CONH– bridge allows the PTZ fragment sited a little far from the pyridine ring, the distance between Re and S is 10.78 Å, Re and N is 8.59 Å, and the Re–N–S angle is 130.03°; whereas in the model of **1b**, the distance between Re and S is 8.55 Å, Re and N is 7.15 Å, and the Re–N–S angle is 107.11°. Electron delocalization can be observed on the pyridine ring in the HOMO orbital of **1a**, whereas there is no delocalization existing in the case of **1b**. Furthermore, not much difference can be observed for their LUMO orbitals, that is, the configuration of **1a** could facilitate ET through space just like that of **1b**. The conclusion is that

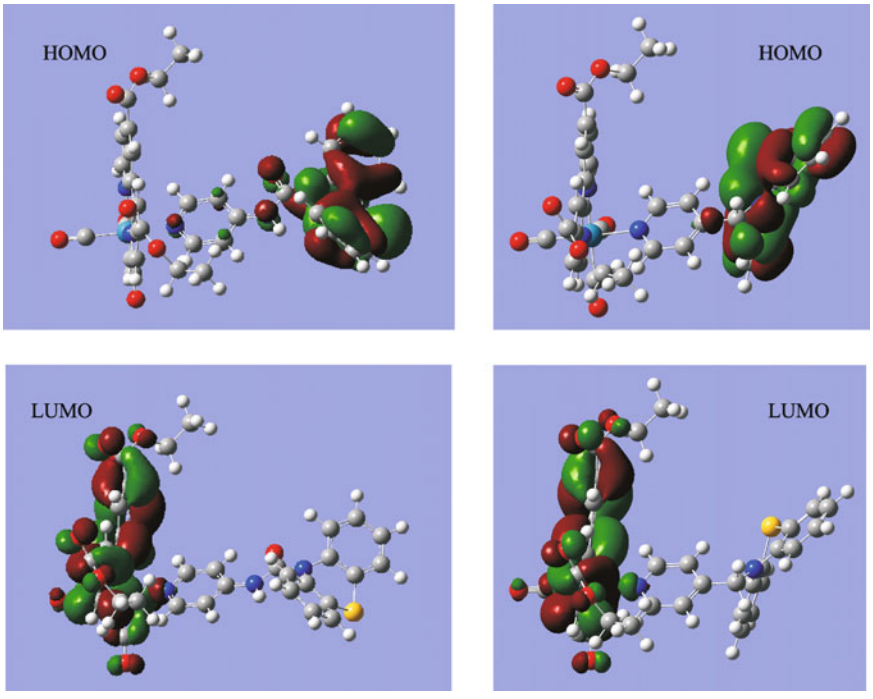

Figure 5 HOMO and LUMO orbital of **1a** (left) and **1b** (right) with Re-, N-, O-, and S-atom in dark cyan, blue, red, and yellow color, respectively.

intramolecular ET depends heavily on the linking bridge in complex **1**. Much detailed investigation is still ongoing in our laboratory.

4 Conclusions

Intramolecular ET depends mainly on the linking bridge in complex **1**, the Re^{+}-PTZ + MV^{2+} system can build a good model for studying the ET process since PTZ radical is relatively stable and can be easily observed by transient absorption and time resolved absorption spectrometry. Our result provides useful information on the designation of novel ET system in the future.

Acknowledgements The work was supported by State Key Laboratory of Fine Chemicals, Dalian University of Technology, the Education Ministry and National Natural Science Foundation of China (Grant Nos. 20872012, 20071108, 707016, 20706008, and 20725621), the Education Department of Liaoning Province (Grant No. 2008S040), Specialized Research Fund for the Doctoral Program of Higher Education (Grant No. 200801411004), Program for Changjiang Scholars and Innovative Research Team in University (Grant No. IRT0711), and the Open Research Fund of State Key Laboratory of Bioelectronics, Southeast University.

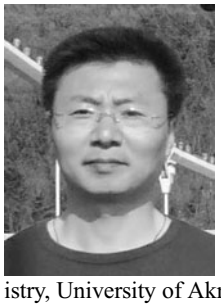

Shiguo SUN got his Ph.D. degree in the field of applied chemistry from Dalian University of Technology in 2003. He then did postdoc researches in Department of Chemistry, Stockholm University (2004–2005) and Department of Chemistry, Royal Institute of Technology (KTH), Stockholm, Sweden (2005–2006). He worked as a research scientist in Department of Chemistry, University of Akron in 2006–2007. Since 2006, he has been an associate professor at State Key Laboratory of Fine Chemicals, Dalian University of Technology. His research interest is functional molecule with special light or electrochemistry properties.

References

1. Sun, L.; Hammarstrom, L.; Åkermark, B.; Styring, S., *Chem. Soc. Rev*. **2001**, *30*, 36–49
2. Alstrum-Acevedo, J.H.; Brennaman, M.K.; Meyer, T.J., *Inorg. Chem*. **2005**, *44*, 6802–6827
3. Sjödin, M.; Styring, S.; Åkermark, B.; Sun, L.; Hammarstrom, L., *J. Am. Chem. Soc*. **2000**, *122*, 3932–3936
4. Johansson, A.; Abrahamsson, M.; Magnuson, A.; Huang, P.; Mårtensson, J.; Styring, S.; Hammarström, L.; Sun, L.; Åkermark, B., *Inorg. Chem*. **2003**, *42*, 7502–7511
5. Xu, Y. H.; Eilers, G.; Borgström, M.; Pan, J. X.; Abrahamsson, M.; Magnuson, A.; Lomoth, R.; Bergquist, J.; et al., *Chemistry* **2005**, *11*, 7305–7314
6. McEvoy, J. P.; Brudvig, G. W., *Chem. Rev*. **2006**, *106*, 4455–4483
7. Mayer, J. M.; Rhile, I. J.; Larsen, F. B.; Mader, E. A.; Markle, T. F.; DiPasquale, A. G., *Photosynth. Res*. **2006**, *87*, 3–20
8. Kosower, E. M.; Cotter, J. L., *J. Am. Chem. Soc*. **1964**, *86*, 5524–5527
9. Watanabe, T.; Honda, K., *J. Phys. Chem*. **1982**, *86*, 2617–2619
10. Ghanem, R.; Xu, Y.; Pan, J.; Hoffmann, T.; Andersson, J.; Polivka, T.; Pascher, T.; Styring, S.; et al., *Inorg. Chem*. **2002**, *41*, 6258–6266
11. Argazzi, R.; Bignozzi, C. A.; Heimer, T. A.; Castellano, F. N.; Meyer, G. J., *J. Phys. Chem. B* **1997**, *101*, 2591–2597
12. Chen, P.; Duesing, R.; Graff, D. K.; Meyer, T. J., *J. Phys. Chem*. **1991**, *95*, 5850–5858
13. Chen, P.; Westmoreland, T. D.; Danielson, E.; Schanze, K. S.; Anthon, D.; Neveux, P. E. Jr; Meyer, T. J., *Inorg. Chem*. **1987**, *26*, 1116–1126
14. Bates, W. D.; Chen, P.; Dattelbaum, D. M.; Jones, W. E.; Meyer, T. J., *J. Phys. Chem. A* **1999**, *103*, 5227–5231
15. Shaver, R. J.; Perkovic, M. W.; Rillema, D. P.; Woods, C., *Inorg. Chem*. **1995**, *34*, 5446–5454
16. Hagfeldt, A.; Grätzel, M., *Acc. Chem. Res*. **2000**, *33*, 269–277
17. Berg, K. E.; Tran, A.; Raymond, M. K.; Abrahamsson, M.; Wolny, J.; Redon, S.; Andersson, M.; Sun, L.; et al., *Eur. J. Inorg. Chem*. **2001**, *4*, 1019–1029
18. Garelli, N.; Vierling, P. J., *J. Org. Chem*. **1992**, *57*, 3046–3051
19. MacQueen, D. B.; Schanze, K. S., *J. Am. Chem. Soc*. **1991**, *113*, 7470–7479
20. Yang, L.; Ren, A. M.; Feng, J. K.; Liu, X. D.; Ma, Y. G.; Zhang, H. X., *Inorg. Chem*. **2004**, *43*, 5961–5972
21. Frisch, M. J., et al., Gaussian 09, Revision C 02, Gaussian, Inc., Wallingford, CT, 2009